One for all – Human kidney Caki-1 cells are highly susceptible to infection with corona- and other respiratory viruses

Daniels A.[1,2,◊], Fletcher S. [1,◊], Kerr H.[1], Kratzel A.[3,4], Kriplani N.[1,♠], Craig N.[1], Hastie J.C.[5], Digard P.[1], Davies P.[5], Thiel V.[3,4], Tait-Burkard C.[1]*

[1]The Roslin Institute, Royal (Dick) School of Veterinary Studies, University of Edinburgh, Easter Bush, Midlothian, United Kingdom.

[2]Infection Medicine, University of Edinburgh, Little France Crescent, United Kingdom.

[3]Institute of Virology and Immunology (IVI), Bern, Switzerland.

[4]Department of Infectious Diseases and Pathobiology, Vetsuisse Faculty, University of Bern, Bern, Switzerland.

[5]Medical Research Council Protein Phosphorylation and Ubiquitylation Unit, College of Life Sciences, University of Dundee, Dundee, United Kingdom.

◊ contributed equally

♠Currently: Milteny Biotec, United Kingdom

*Corresponding author: christine.burkard@roslin.ed.ac.uk

Abstract

Despite the vast increase in research activity in the coronavirus field over the past two years, researchers are still heavily reliant on non-human cells, for example Vero E6, highly heterogeneous or not fully differentiated cells, such as Calu-3, or not naturally susceptible cell lines overexpressing receptor ACE2 and other accessory factors, such as TMPRSS2. Complex cell models, such as primary cell-derived air-liquid interface epithelial models are highly representative of human tissues but are expensive and time-consuming to develop and maintain and have limited suitability for high-throughput analysis. *In vitro* investigations of host-pathogen interactions of viruses is highly reliant on suitable cell and tissue culture models and results are only as good as the model they have been validated in.

Here, we show the use of a highly characterized human kidney cell line, Caki-1, for infection with three human coronaviruses: *Betacoronaviruses* severe acute respiratory syndrome coronavirus-2 (SARS-CoV-2) and Middle Eastern respiratory syndrome coronavirus (MERS-CoV) and *Alphacoronavirus* human coronavirus 229E (hCoV-229E). Caki-1 cells show equal or superior susceptibility to all three coronaviruses when compared to other commonly used cells lines for the cultivation of the respective virus. Furthermore, we used a panel of antibodies generated against 21 SARS-CoV-2-encoded proteins to identify their location in the infected Caki-1 cells using immunocytochemistry. Most importantly, Caki-1 cells are also susceptible to two other respiratory viruses, Influenza A virus and RSV, making them an ideal model for cross-comparison of not only a broad range of coronaviruses but respiratory viruses in general.

Introduction

Coronaviruses are a family of enveloped, positive-sense RNA viruses within the order *Nidovirales* that are split into four genera, alpha-, beta-, delta-, and gamma- coronaviruses. *Alpha*- and *Betacoronaviruses* mainly infect mammalian hosts while the *Delta*- and *Gammacoronaviruses* primarily infect avian hosts (1). Four members of the human coronaviruses (hCoV) cause mild, cold-like, primarily upper respiratory tract symptoms upon infection: *Alphacoronaviruses* -229E and -NL63 and *Betacoronaviruses* -HKU1 and -OC43. On three occasions in the last 20 years, zoonotic transmission events in the *Betacoronavirus* genus lead to epidemic and pandemic disease outbreaks with higher severity pathologies: Severe acute respiratory syndrome coronavirus (SARS-CoV) in 2002-2003 (2), Middle Eastern respiratory syndrome coronavirus (MERS-CoV) that was first reported in 2012-ongoing (3), and most recently the causative agent of the coronavirus disease 2019 (COVID-19) pandemic that was first described towards the end of 2019, SARS-CoV-2 (4). The potential for future zoonotic events increases as human pressure on nature grows, for example population growth, displacement due to climate change, deforestation, and finding alternative food sources leads to greater contact with wild reservoir species.

Understanding coronavirus infections and host-pathogen interaction is paramount to developing novel antiviral strategies, and to prepare for future epidemics. This makes it imperative to find a robust cell line model that is widely permissive to different coronaviruses to allow for direct comparison and aid future research.

Important criteria for selecting cell lines include species origin, tissue relevance, method of immortalization (i.e. presence of overexpressed viral oncogenes), genetic characterization and karyotype, versatility, and ease of culturing. A number of cell lines were identified as being naturally permissive to SARS-CoV-2, most notably Vero E6, Caco-2, and Calu-3 cells (5). Overexpression of the main entry receptor, angiotensin-converting enzyme 2 (ACE2), sometimes aided by the overexpression of the proteolytic processing factor transmembrane protease, serine 2 (TMPRSS2) was shown to render non-susceptible cell lines permissive to SARS-CoV-2 infection. Although these cell lines are permissive to infection, there are limitations and drawbacks to their use in research. Most notably, Vero E6 cells, which have been shown to be susceptible to many human viruses including influenza A virus (IAV), SARS-CoV, and MERS-CoV, are of the African Green Monkey (*Chlorocebus aethiops*) species origin, making them a less clinically relevant model. More importantly, they are deficient in type I interferon production due to a large deletion in the genome (6). Tissue culture adaptation mutations and attenuation in the viral genome, such as the loss of the S1/S2 furin-cleavage site in SARS-CoV-2 spike (S), have been observed when the virus was passaged on Vero E6 cells (7). Although the other notable cell lines commonly used to study

80 SARS-CoV-2 are of human origin, viral titers obtained from Calu-3 and Caco-2 are lower than in
81 Vero E6 cells(8). Furthermore, Calu-3 and Caco-2 cells are heterogeneous populations of not fully
82 differentiated cells, which means that consistency in cells can vary based on culturing methods,
83 as well as some people reporting difficulties culturing, especially Calu-3 cells. Other, less explored
84 cell lines were shown to be susceptible to high-titer SARS-CoV-2 infection, such as the breast
85 cancer cell line CAL-51 (5),

86 The need for consistent and comparable cell lines has again been highlighted by the results from
87 several genome-scale CRISPR knock-out studies investigating host factors during SARS-CoV-2
88 infection. The screens used different cell lines including Vero E6 (9), A549-ACE2 (10, 11), Huh7.5
89 (12), or a clone of Huh7.5 modified to overexpress both ACE2 and TMPRSS2 (Huh7.5.1-ACE2-
90 IRES-TMPRSS2) (13). Of these studies, ACE2 and cathepsin L (CTSL) were the only gene hits to
91 overlap across all screens, and the most overlap was observed between screens utilizing the same
92 cell lines (10, 11) or clonal variants of a cell line (12, 13). Although this suggests that there is
93 reproducibility when using the same cell line, some cell lines modified for overexpression of
94 cellular receptors have limited use for cross-comparison studies between viruses. For instance,
95 while A549-ACE2 cells would be sufficient for comparing SARS-CoV and -2, both of which utilize
96 ACE2, they could not be used to compare to other coronaviruses, such as hCoV-229E utilizing
97 alanyl aminopeptidase (ANPEP) or MERS-CoV utilizing dipeptidyl peptidase 4 (DPP4) during
98 entry. Huh7.5 cells and their derivatives are more useful as they are naturally infected by both
99 hCoV-229E, and MERS-CoV as they express a wide range of cell surface receptors so they could
100 be utilized in pan-coronavirus studies. However, they are not very robust and exhibit extreme
101 cytopathic effect upon infection which limits what can be studied within these cells.

102 As the cell lines that have been predominantly used to study SARS-CoV-2 have limitations,
103 including poor infection with our clinical isolates of SARS-CoV-2, we aimed to find an adherent
104 cell line that was both easy to transfect and naturally permissible to SARS-CoV-2. As the human
105 protein ATLAS identifies the kidney as being a high region of ACE2 expression, and pathology has
106 identified SARS-CoV-2 infection within the kidneys of infected patients, we identified a human
107 cell line isolated from a male clear cell carcinoma patient, Caki-1 (ATCC HTB-46), which has been
108 previously used in cancer and toxicology studies. It has been well characterized through a number
109 of loss-of-function screens and omics characterizations, as well as having data on drug
110 sensitivities through the use of compound viability screens. A complete list of datasets can be
111 found through the depmap portal (https://depmap.org/portal/cell_line/ACH-000433). Although
112 Caki-1 cells have previously been reported to be permissive to two members of the family
113 *Poxviridae*, myxoma virus (14) and Tanapoxvirus (15), they have not been reported to have been
114 tested for infection with an RNA virus.

115 Here we describe the successful infection of Caki-1 cells when challenged with SARS-CoV-2,
116 MERS-CoV, and hCoV-229E. All viruses were replicated to similar or improved levels compared
117 to commonly used cell lines. A panel of antibodies raised in sheep against 21 of the known
118 proteins encoded by SARS-CoV-2 have been used to study their cellular location during the SARS-
119 CoV-2 replication. We found good expression of receptors, interferon competence and
120 susceptibility to gene knockdown in Caki-1 cells. Furthermore, two clinically important RNA
121 respiratory viruses, influenza A virus (IAV, order *Articulavirales*), and respiratory syncytial virus
122 (RSV, order *Mononegavirales*) were also found to infect Caki-1 cells to comparable levels of
123 commonly used cell lines in infection with the respective viruses.

124

125 **Results**

126 To compare the differences between infection in Caki-1 cells and the typical amplification cell line
127 for each coronavirus, time courses of infection were performed for SARS-CoV-2, including
128 variants of concern (VOCs), MERS-CoV, and hCoV-229E.

129 **Caki-1 cells show matching or improved infectability with SARS-CoV-2 compared to Vero**
130 **E6 cells**

131 Cells were infected with SARS-CoV-2 D614G or VOCs alpha, delta, or omicron (BA.1) to investigate
132 how the growth profile differed between clinical isolates from early stages of the pandemic
133 through to the current predominant variant, omicron (Results

134 A). Cells at confluence were inoculated with MOIs 0.1, 1, or 10 as determined by endpoint titration
135 on Vero E6 cells, except for omicron, which was titrated on Caki-1 cells. Following media
136 replacement at 1.5 hours post inoculation (hpi), supernatant samples were collected and viral
137 particles determined by direct lysis against a standard curve of known titer samples. The
138 European "Original" strain EDB-2 showed a similar replication pattern in Caki-1 and Vero E6 cells,
139 at all MOIs, with both reaching a plateau at 24 hpi at a relative $TCID_{50}$/ml of ~10^7 and maintaining
140 that value until the 120 hpi time point. There was little difference in the log phase for EDB-2
141 between the cell lines and between MOIs, although the Vero E6 cells show greater variation across
142 the time points than Caki-1 cells where variation decreases as the MOI increases. For the alpha
143 variant, first detected in November 2020, using strain EDB-α-1, the replication in Vero E6 cells
144 starts to diverge away from the log curve for all MOIs, with the MOI of 0.1 lagging slightly behind,
145 the curve flattens into a more linear phenotype peaking at 96 hpi with a relative $TCID_{50}$/ml in the
146 low 10^6 region. Contrastingly, viral replication in Caki-1 cells still shows a logarithmic phenotype,
147 with stratification between the MOIs through the log phase before all plateauing at 48 hpi with a
148 relative $TCID_{50}$/ml maintained at ~10^7. The delta variant, which emerged in late 2020, using
149 strain EDB-δ-1 did not replicate as well as either previous variant overall and shows a more linear
150 phenotype, similar to the EDB-α-1 variant in Vero E6, in both Vero E6 and Caki-1 cells. In both
151 cell lines replication plateaus at 72 hpi up to a relative 2-3x10^6 $TCID_{50}$/ml by 96 hpi. For EDB-δ-1
152 the increase in viral titer across the entire time course, in both cell lines, was only two logs
153 whereas in Caki-1 cells for EDB-2 and EDB-α1 the fold change was five logs. The last variant of
154 concern, omicron, was detected in December 2021 with new subvariants emerging since. Here,
155 using EDB-o-BA.1-10, we saw very poor infection in Vero E6 cells, barely increasing by a single
156 log across 120 hours, and even showing a drop off in titer at 120 hpi as the virus decays. The virus
157 was then also not originally isolated on Vero E6 as it could not be grown on the cell line but rather
158 on Caki-1. In Caki-1 cells, we see a phenotype which is comparable to the original EDB-2 strain
159 with a log phase peaking at 24 hpi and stratification between the different MOIs. Once EDB-o-

160 BA.1-10 reaches a plateau in Caki-1 cells at a relative $TCID_{50}$/ml of ~10^6, it remains steady with
161 very little variation for the remainder of the time course. Viral replication of EDB-o-BA.1-10 in
162 Caki-1 is reaching higher particle levels compared to Vero E6 cells. As the virus evolved, it
163 remained accustomed to replicating in the Caki-1 cells whilst a progressively weaker infection is
164 established in Vero E6 cells, apart from EDB-δ-1, which does not replicate well in either cell line.

165 **Caki-1 cells show improved infectability with MERS-CoV and hCoV-229E compared to**
166 **Huh-7**

167 Since Caki-1 cells showed a good permissibility and infection with SARS-CoV-2, other
168 coronaviruses were tested to determine if Caki-1 cells could be used as a pan-coronavirus model.
169 To this end, the highly pathogenic beta coronavirus, MERS-CoV, and the less pathogenic, common
170 cold alpha coronavirus, hCoV-229E, were tested for replication in Caki-1 cells (Results

171 B+C). The traditional cell line for both these viruses is Huh-7.

172 For MERS-CoV infection, both Caki-1 and Huh-7 cells were inoculated at indicated virus
173 concentrations as determined on Huh-7 cells. After 2 h, inoculum was replaced and samples taken
174 at indicated time points. Infectious virus produced was assessed by endpoint titration on Huh-7
175 cells. In initially infected Huh-7 cells, the viral titer for MERS-CoV rose rapidly to 24 hpi and peaks
176 here for an MOI of 1, but is slightly delayed for the lower MOIs, peaking at 48 hpi for 0.1 and 0.01
177 (Figure 1B). At all MOIs, a peak of ~$1.2x10^7$ $TCID_{50}$/ml titer is achieved. After peaking, a rapid
178 decline is observed for every MOI, crashing down to 10^4 $TCID_{50}$/ml by 96 hpi. Whilst the
179 exponential phase in Caki-1 cells shows initial similarities to Huh-7 the viral titers plateau at 48
180 hpi for all MOIs. By that time, the cells have managed to support the virus to reach a $TCID_{50}$/ml of
181 ~$2.1x10^9$, which is two logs higher than Huh-7 cells in any condition. Whilst MOIs of 0.1 and 1
182 show a decreasing titer to ~10^5 $TCID_{50}$/ml, MOI 0.01 infectious titers remain high up to 96 hpi.
183 Caki-1 cells show a strong potential with MERS-CoV to be used as a new model system for growing
184 the virus, higher titers are achieved with lower infection concentrations and the titers do not
185 decrease with cell apoptosis as Caki-1 cells can robustly support the infection to its completion.

186 To test whether Caki-1 cells are permissive to hCoV-229E, a GFP virus was used to measure
187 infection throughout the course of infection using relative fluorescence of GFP as a proxy for viral
188 replication rather than $TCID_{50}$/ml (Results

189 C). Caki-1 and Huh-7 cells were inoculated at indicated virus concentrations as determined on
190 Huh-7 cells. After 1.5 h, inoculum was replaced and plates returned to an incubating plate reader
191 for analysis. The level of fluorescence achieved by both cell lines when infected is comparable to
192 each other, but in Caki-1 cells, we see a quicker and more exaggerated log phase, reaching plateau
193 at roughly 40 hpi, about 10 h before Huh-7 cells. There is also a difference in the lower MOI (0.1),

194 which only achieves a plateau fluorescence value around 5,000 RFU in the Huh-7 cells, a >2-fold
195 reduction compared to Huh-7 cells infected at an MOI of 1, while Caki-1 cells plateau around 8,500
196 RFU, only 2,000 RFU lower than the MOI of 1 and within the margin of error. The Caki-1 cells also
197 show an observable difference of GFP distribution and brightness when compared to Huh-7 cells.
198 Caki-1 cells produce a more uniform phenotype, with less background fluorescence, the GFP is
199 expressed to a greater extent in infected cells, and it takes longer for the cells to round up and lift
200 off the plate. Huh-7 cells generally express the GFP very weakly and in a more punctate fashion,
201 lifting off the plate very early on in infection, making fluorescence readings difficult and
202 inaccurate (data not shown).

203 **Only around 50% of Caki-1 cells get infected by SARS-CoV-2 showing potential of selection**
204 **for even more susceptible subpopulations**

205 To gain greater insight into the infection in Vero E6 cells compared to the more heterogeneous
206 Caki-1 cells, we inoculated the cells at different MOIs (determined on Vero E6 cells) and assessed
207 infection following a single-round infection at 17 hpi through staining for intracellular N protein
208 and analysis by flow cytometry (Figure 1D). For all MOIs analyzed, the level of infected Caki-1
209 cells is roughly half of the infected Vero E6 cells. The Vero E6 population manages to reach up to
210 ~85.3% infected cells by 17 hpi at an MOI=10 and within the margin of error compared to MOI=1,
211 whereas the Caki-1 reach an infection ~46.8%. Another cell line used for SARS-CoV-2 research is
212 Calu-3, an epithelial lung adenocarcinoma cell line with heterogeneous ACE2 expression. The
213 percentage of infected cells remains low in the wild-type Calu-3 population, reaching 6% infection
214 when inoculated at MOI=10 by 24 hpi, and only increasing by 0.8% after 48 hpi. But Calu-3's
215 which have been enriched for high expression of ACE2 through staining, fluorescence activated
216 cell sorting, and expansion, showed a marked increase in percentage of infection cells, reaching
217 21% at an MOI=0.1 at 24 hpi and roughly 50% at all MOIs at 48 hpi. Whilst Calu-3 cells take longer
218 to establish an infection, if enriched with ACE2 they are capable of reaching infection levels
219 similar to Caki-1 cells although this is most likely through a multi-round infection unlike the
220 single-round infection in Caki-1 cells at 17 hpi.

221 Caki-1 cells are permissible to all tested coronaviruses and in EDB-o-BA.1-1, MERS-CoV and
222 hCoV-229E, show a stronger infection than in Vero E6 and Huh7 cells respectively. As SARS-CoV-
223 2 VOCs emerged, Caki-1 cells have become a better infection model than the Vero E6 cells, except
224 for EDB- δ-1, which universally is attenuated in cell culture. They also provide a good replication
225 model for other coronaviruses and can outperform the standard Huh-7 cells.

226 **Localization of viral proteins in Caki-1 cells during replication may pinpoint towards**
227 **functionality**

228 To gain a greater understanding of SARS-CoV-2 infection, antibodies were developed against all
229 major proteins encoded by the SARS-CoV-2 genome (Figure 2A) by the University of Dundee
230 MRC-Protein Phosphorylation Unit (16). Caki-1 cells infected at a MOI=1 with SARS-CoV-2-EDB-2
231 were fixed at 16 hpi and stained with antibodies targeting most non-structural proteins and the
232 known open reading frames in the "structural" section of the genome. A compromise was found
233 using the antibodies, which had varying stock concentrations, at 1 in 200. Concentrations are
234 therefore not comparable and for specific use of an antibody, we recommend further
235 optimization. Further details may be found in the materials and methods section and table 1.
236 Confocal images were acquired as z-stacks on a Zeiss LSM 880 (Airyscan) without making use of
237 the airyscan function. Imaging conditions were set for each uninfected, stained background cell
238 with the matching primary antibody. Images depict a maximum projection of the z-stack.

239 Of the open reading frame (ORF)2-10 encoded proteins, ORF3a and b, ORF8 and ORF9 (N) show
240 the strongest signals above background, but all SARS-CoV-2 ORF antibodies show specific
241 staining beyond background (Figure 2B). The spike receptor binding domain (S RBD), ORF2,
242 shows vesicle-like punctate throughout the cytoplasm with a slight enrichment in the enlarged
243 perinuclear space in some cells. There is little staining for S at the plasma membrane, which is in
244 agreement with previous findings showing that only roughly 20% of coronavirus S protein may
245 be found at the plasma membrane in the presence of M (17, 18). The viroporin ORF3a, shows
246 punctate staining with concentration around the perinuclear space, this agrees with current
247 SARS-CoV literature and reports of it being involved in autophagy, localizing to the lysosomes (19,
248 20). Although there is some background staining in uninfected Caki-1 cells for ORF3a, the staining
249 in the infected control is significantly stronger and background signal is non-specifically localized
250 indicating non-specific background binding that may be optimized using different staining
251 conditions. The small ORF3b protein, which acts as a potent interferon antagonist, localizes in the
252 distal cytoplasm with some vesicular patterning. ORF3b also shows staining at the plasma
253 membrane particularly along actin filaments. This agrees with reports for SARS-CoV of it being a
254 multi-localized protein due to its shuttling behavior (21). Co-localization studies with known
255 interaction partners, such as IRF3, may shed further light into the role of ORF3b (22). SARS-CoV-
256 2 ORF7a and ORF7b are type-I transmembrane proteins also involved in antagonism of the
257 interferon response. Both are expressed and retained intracellularly. Background staining is
258 observed for both these antibodies in the uninfected Caki-1 cells, but the fluorescence is stronger
259 in the infected cells. ORF7a shows vesicular, diffuse localization, whilst ORF7b is concentrated in
260 the perinuclear space with some plasma membrane staining. Little is known about the function
261 of the two proteins, but for example ORF7b was shown to be incorporated into SARS-CoV
262 particles (23). The protein encoded by the SARS-CoV-2 ORF8 gene is unique to SARS-CoV-2

263 containing a predicted Ig-like fold, which can interact with a variety of host proteins involved in
264 ER-associated degradation. Caki-1 cells show a strong staining with no background in the
265 uninfected cells, and we see a vesicular staining with a concentration towards the plasma
266 membrane in agreement with the existing literature showing secretion of ORF8 (24). ORF9, the
267 nucleocapsid protein (N), shows localization to the replication-transcription complex in the
268 perinuclear space, where it aids packaging of the viral genome into a ribonucleoprotein particle.
269 Staining for N is abundant across the cell, and even shows a small amount of nuclear staining (the
270 seemingly stronger nuclear staining visible in the image is a consequence of maximum
271 projection). N is also secreted into the extracellular space in larger amounts than ORF8, indicated
272 by some of the vesicular and distal staining (25, 26). An alternative ORF located within the N gene
273 is ORF9b, which plays a role in suppressing innate immunity. ORF9b shows a very diffuse staining
274 across the cell with no background in the uninfected cells. Reports have linked this protein with
275 the mitochondrial membrane (27, 28), and upon close inspection, long punctate networks can be
276 seen within some of the staining, although this is not obvious indicating mitochondrial interaction
277 not to be a primary function of the protein. Most importantly, ORF9b shows clear nuclear
278 localization.

279 The SARS-CoV-2 non-structural proteins (NSPs) are generated through proteolytic cleavage of
280 the ORF1a and ORF1ab polyproteins. Of these, NSPs 3, 8, 10 and 16 gave the clearest staining.
281 However, some NSPs showed very little specific staining, primarily NSP9 for which no staining
282 could be seen in infected Caki-1 cells (Figure 3). The N-terminal cleavage products NSP1 and NSP2
283 are conserved across the coronavirus family and are both involved in halting host translation
284 (29). Whilst NSP1 shows very sparse staining in very distinct punctae throughout the cytosol,
285 staining for NSP2 is concentrated around the perinuclear space. NSP3 is responsible for cleavage
286 of NSP1, NSP2, and NSP3 from the N-terminal region of the polyproteins (30), and shows
287 widespread, punctate staining. Some cells, possibly at an earlier stage in their infection cycle,
288 show a more perinuclear focused staining, likely co-localizing with the replication transcription
289 complex (RTC). The main proteinase NSP5 shows a very strong perinuclear, likely RTC,
290 phenotype. The replicase (NSP8) exhibits strong perinuclear staining showing big spots of
291 protein staining, defined by its role in the RTC (31). NSP8 also shows some nuclear staining,
292 however, since there is some background nuclear staining it is unlikely this is a real signal. The
293 growth-factor-like protein NSP10, which serves as a stimulatory factor for NSP14-ExoN (32),
294 shows broadly distributed punctate staining with some localization to the plasma membrane and
295 although the staining for NSP14 is not as strong, it demonstrates a similar pattern but with no
296 membrane localization. NSP11_12, the latter being the RNA-dependent-RNA-polymerase, shows
297 staining localizing to the RTC, as do the helicase NSP13, the endoribonuclease NSP15. There may

298 be some staining for NSP13 in the nucleus. NSP16, a methyltransferase, shows nuclear staining
299 and punctate staining throughout the cytosol indicating vesicular localization, and potentially
300 some secretion (33).

301 **Caki-1 cells show expression of receptors linked to SARS-CoV-2 and other human**
302 **coronaviruses**

303 To further understand the suitability of Caki-1 cells for infection assays and to account for the
304 high permissibility to many coronaviruses, receptor expression profiling, interferon competence
305 and siRNA knockdowns were conducted. The receptors/entry proteins for SARS-CoV-2,
306 MERS-CoV and hCoV-229E, were checked for mRNA quantity by RT-qPCR, and normalized
307 against a housekeeping gene (RRN18S) (Figure 1**: Time course assays in coronaviruses**
308 **comparing the most commonly used cell line with Caki-1.** For all graphs: circle points = MOI
309 10, square points = MOI 1, triangle points = MOI 0.1, diamond points = MOI 0.01, and the darker
310 the color the higher the MOI, error bars indicate +/- SEM. [A] Time course infection of SARS-CoV-
311 2 variants on Vero E6 and Caki-1 cells, biological n=3x3. Measured through RT-qPCR for the SARS-
312 CoV-2 N gene in the supernatant, samples taken at 0, 6, 16, 24, 48, 72, 96 and 120 hpi at MOIs of
313 10, 1 and 0.1. [B] Time course infection of MERS-CoV on Huh-7 and Caki-1 cells, biological n=3x3,
314 measured through TCID50 on Huh-7 cells. Samples taken at 24h intervals until 96hpi. [C] GFP
315 time course of infection for hCoV-229E on Huh-7 and Caki-1 cells, measured from 0 hpi to 78 hpi
316 in 6 h intervals, with fluorescence as a proxy for viral replication, biological n=3x3. [D]
317 Fluorescence-activated cell sorting to determine the percentage of infected SARS-CoV-2 cells in
318 Vero E6, Caki-1, Calu-3 and Calu-3-ACE2 cells. Vero E6 and Caki-1 cells were fixed at 17 hpi,
319 stained for intracellular SARS-CoV-2 N protein and sorted for fluorescent cells, biological n=3x3.
320 The same was conducted for Calu-3 and Calu-3-ACE2 cells at 24 hpi and 48 hpi, biological n=3x3.

321 A). NRP1 (SARS-CoV-2 attachment), ANPEP (hCoV-229E receptor) and DPP4 (MERS-CoV
322 receptor) all showed a similar level of expression in Caki-1 cells demonstrating that they are
323 actively being expressed. Levels of around 1,000-fold lower expression than a housekeeping gene
324 are in alignment with expression levels previously determined in lung (e.g. DPP4 (34)). ACE2
325 (SARS-CoV-2 receptor) and TMPRSS2 (one of the SARS-CoV-2 spike modifying proteases) had a
326 relative lower amount of mRNA than the other factors, but this pattern correlates with expression
327 of these proteins in nasal epithelial cells (35), perhaps providing an indication as to why they are
328 so readily infectable with SARS-CoV-2.

329 **Caki-1 cells can be readily transfected with siRNA**

330 To confirm Caki-1 cells are suitable cells in which to perform transfection experiments the effect
331 of siRNA transfection targeting known entry factors of SARS-CoV-2 was examined by reading viral
332 release 96 h post transfection (hpt) and 24 hpi (Figure 4B). A panel of genes implicated in

333 SARS-CoV-2 entry (ACE2, TMPRSS2, NRP1, CTSB, CTSL), and a virus specific gene (SARS-CoV-2
334 N) were knocked down before infection with EDB-2 at 72 hpt. All genes showed a significant
335 (****p<0.0001) reduction in replication compared to non-targeting siRNA, with SARS-CoV-2 N
336 and NRP1 showing the strongest phenotypes with a relative replication compared to the
337 non-targeting control of 8 and 9% respectively. Knockdown of CTSB had the least effect on viral
338 replication, only causing a 50% reduction in released virus, followed by TMPRSS2 at 24.7%
339 relative replication. The viability of the Caki-1 cells after knockdown was measured by
340 fluorescence created through mitochondrial metabolism as a proxy for cell viability. There was
341 no difference to cell viability after knockdown of any of these genes. Neither was there any effect
342 on cell viability due to being treated with the transfection reagent (Mock). This shows that Caki-1
343 cells can be transfected successfully and that it results in the desired effect on viral replication,
344 they can also tolerate the transfection reagent without a reduction in cell viability. Knockdowns
345 were validated by RT-qPCR and showed at least 80% reduction in mRNA (data not shown).

346 **Caki-1 cells are interferon competent**

347 Many cancer cells lines are deficient in their interferon response, especially Vero E6 cells, which
348 lack the ability to produce interferon through a large deletion in their genome (6). This can be
349 detrimental for studying a fully comprehensive viral replication cycle, as close to natural infection
350 as possible in a cancer cell line. It often also drives viral adaptation over serial passaging of field
351 isolates. To assess the interferon response in Caki-1 cells, and therefore their suitability as a good
352 infection model for SARS-CoV-2, we stimulated them with Poly I:C and LPS and measured their
353 IFNα/β output by HEK-Blue IFNα/β assay (Figure 1**: Time course assays in coronaviruses**
354 **comparing the most commonly used cell line with Caki-1.** For all graphs: circle points = MOI
355 10, square points = MOI 1, triangle points = MOI 0.1, diamond points = MOI 0.01, and the darker
356 the color the higher the MOI, error bars indicate +/- SEM. [A] Time course infection of SARS-CoV-
357 2 variants on Vero E6 and Caki-1 cells, biological n=3x3. Measured through RT-qPCR for the SARS-
358 CoV-2 N gene in the supernatant, samples taken at 0, 6, 16, 24, 48, 72, 96 and 120 hpi at MOIs of
359 10, 1 and 0.1. [B] Time course infection of MERS-CoV on Huh-7 and Caki-1 cells, biological n=3x3,
360 measured through TCID50 on Huh-7 cells. Samples taken at 24h intervals until 96hpi. [C] GFP
361 time course of infection for hCoV-229E on Huh-7 and Caki-1 cells, measured from 0 hpi to 78 hpi
362 in 6 h intervals, with fluorescence as a proxy for viral replication, biological n=3x3. [D]
363 Fluorescence-activated cell sorting to determine the percentage of infected SARS-CoV-2 cells in
364 Vero E6, Caki-1, Calu-3 and Calu-3-ACE2 cells. Vero E6 and Caki-1 cells were fixed at 17 hpi,
365 stained for intracellular SARS-CoV-2 N protein and sorted for fluorescent cells, biological n=3x3.
366 The same was conducted for Calu-3 and Calu-3-ACE2 cells at 24 hpi and 48 hpi, biological n=3x3.

367 C). Stimulation with a transfection reagent only (DF1) induced a small response, comparable to
368 cells cultured in media containing Poly I:C. Caki-1 cells only showed a very small response to LPS
369 stimulation, comparable to other stimulant addition. However, when Poly I:C was transfected to
370 mimic a viral infection, IFN α/β production rose dramatically from 0.0004 μg/ml for DF1 only to
371 0.2 μg/ml for 1 μg/ml Poly I:C (****$p<0.0001$) and 0.08 μg/ml for 10 μg/ml Poly I:C (***$p<0.001$).
372 None of the other conditions provided a significant difference from untreated. This demonstrates
373 that Caki-1 cells can mount a competent interferon response, and so, in assays which investigate
374 interferon pathways in viral replication, and any other host-pathogen interactions, they would
375 provide a complete picture of viral replication.

376 **Caki-1 cells are broadly susceptible to infection with other respiratory viruses RSV and IAV**
377 To determine whether Caki-1 cells are also permissible to infection with other respiratory viruses
378 not in the coronavirus family, they were infected with IAV (H1N1 vaccine strain A/Puerto
379 Rico/8/1934) PR8 and RSV and compared to the standard cell line used to replicate these viruses.
380 In a trypsin-dependent infection with IAV PR8 Caki-1 cells showed replication equal to MDCK
381 cells when infected with an MOI=0.01. No infection was observed in a trypsin-independent
382 infection (data not shown). There was no significant difference at all time points apart from 12
383 hpi where the MDCKs show a higher viral titer by 32,800 pfu/ml, with both cell lines reaching
384 10^{11} pfu/ml by 48 hpi (Figure 1**: Time course assays in coronaviruses comparing the most**
385 **commonly used cell line with Caki-1.** For all graphs: circle points = MOI 10, square points =
386 MOI 1, triangle points = MOI 0.1, diamond points = MOI 0.01, and the darker the color the higher
387 the MOI, error bars indicate +/- SEM. [A] Time course infection of SARS-CoV-2 variants on Vero
388 E6 and Caki-1 cells, biological n=3x3. Measured through RT-qPCR for the SARS-CoV-2 N gene in
389 the supernatant, samples taken at 0, 6, 16, 24, 48, 72, 96 and 120 hpi at MOIs of 10, 1 and 0.1. [B]
390 Time course infection of MERS-CoV on Huh-7 and Caki-1 cells, biological n=3x3, measured
391 through TCID50 on Huh-7 cells. Samples taken at 24h intervals until 96hpi. [C] GFP time course
392 of infection for hCoV-229E on Huh-7 and Caki-1 cells, measured from 0 hpi to 78 hpi in 6 h
393 intervals, with fluorescence as a proxy for viral replication, biological n=3x3. [D] Fluorescence-
394 activated cell sorting to determine the percentage of infected SARS-CoV-2 cells in Vero E6, Caki-
395 1, Calu-3 and Calu-3-ACE2 cells. Vero E6 and Caki-1 cells were fixed at 17 hpi, stained for
396 intracellular SARS-CoV-2 N protein and sorted for fluorescent cells, biological n=3x3. The same
397 was conducted for Calu-3 and Calu-3-ACE2 cells at 24 hpi and 48 hpi, biological n=3x3.

398 D).

399 HEp-2 cells are typically used to expand RSV. Caki-1 and HEp-2 cells were inoculated with a
400 fluorescence reporter virus RSV-A2-GFP. Replication was measured as a proxy by measuring the
401 florescence reporter in an incubating plate reader. For the first time, the replication in Caki-1 cells

402 does not match or outperform replication of RSV in HEp-2 cells (Figure 1**: Time course assays**
403 **in coronaviruses comparing the most commonly used cell line with Caki-1.** For all graphs:
404 circle points = MOI 10, square points = MOI 1, triangle points = MOI 0.1, diamond points = MOI
405 0.01, and the darker the color the higher the MOI, error bars indicate +/- SEM. [A] Time course
406 infection of SARS-CoV-2 variants on Vero E6 and Caki-1 cells, biological n=3x3. Measured through
407 RT-qPCR for the SARS-CoV-2 N gene in the supernatant, samples taken at 0, 6, 16, 24, 48, 72, 96
408 and 120 hpi at MOIs of 10, 1 and 0.1. [B] Time course infection of MERS-CoV on Huh-7 and Caki-
409 1 cells, biological n=3x3, measured through TCID50 on Huh-7 cells. Samples taken at 24h intervals
410 until 96hpi. [C] GFP time course of infection for hCoV-229E on Huh-7 and Caki-1 cells, measured
411 from 0 hpi to 78 hpi in 6 h intervals, with fluorescence as a proxy for viral replication, biological
412 n=3x3. [D] Fluorescence-activated cell sorting to determine the percentage of infected SARS-CoV-
413 2 cells in Vero E6, Caki-1, Calu-3 and Calu-3-ACE2 cells. Vero E6 and Caki-1 cells were fixed at 17
414 hpi, stained for intracellular SARS-CoV-2 N protein and sorted for fluorescent cells, biological
415 n=3x3. The same was conducted for Calu-3 and Calu-3-ACE2 cells at 24 hpi and 48 hpi, biological
416 n=3x3.

417 E). However, the infection in Caki-1 cells outperforms RSV infection in A549 cells through faster
418 and stronger (higher fluorescence) growth (data not shown). The fluorescence from the HEp-2
419 cells (turquoise) reaches 7,000 RFU for MOIs of 1 and 0.1, with 0.1 remaining slightly under
420 MOI=1 for the entire replication cycle (0 hpi – 78 hpi). Although the Caki-1 cells do show a
421 logarithmic replication curve at both MOIs, it is shallow and plateaus by 42 hpi, about 10 h before
422 the HEp-2 cells. The maximum RFU achieved by the hRSV-A2-GFP is ~3,700, about half of the RFU
423 achieved in HEp-2. The variation at the later timepoints has increased compared to HEp-2 cells.
424 No syncytia formation was observed in the Caki-1 cells upon hRSV-A2-GFP infection, but CPE was
425 present at 48 hpi.

426

427 **Discussion**

428 Here we have shown that Caki-1 cells can be used to model infection for a range of respiratory
429 viruses; SARS-CoV-2, CoV-229e, MERS-CoV, IAV, and RSV. With the exception of RSV, they are
430 comparable to or outperform the current preferred cell line for viral production, whilst also
431 providing a naturally permissible environment for the virus to replicate in. They express all the
432 receptors needed for infection with SARS-CoV-2, MERS-CoV, and hCoV-229E, and are responsive
433 to transfection with siRNA without significant cell death. They have a competent interferon
434 response as demonstrated by stimulation with Poly I:C and are also permissive to other
435 respiratory viruses. This makes them a highly useful model for direct comparison of respiratory
436 viruses across one, unmodified (no overexpression) cell line.

437 The natural susceptibility of Caki-1 (human) cells to a range of respiratory viruses, although not
438 a lung cell line, provides them with an advantage over many other cell lines used for viral
439 research. Particularly over the much used Vero E6 cells (African Green Monkey), which, although
440 permissive to many different viruses, do not provide a representative environment for human
441 pathogens. The broad susceptibility of Caki-1 cells to respiratory virus infection allows for their
442 use in comparative studies between viruses. Calu-3 cells, which have been widely used as a lung
443 cell model for SARS-CoV-2, show a very low percentage infection and are difficult to grow.
444 Selection for ACE2 expressing cells (Calu-3-ACE2) through FACS makes the cells more permissive
445 to infection with SARS-CoV-2 and can also enhance growth characteristics through selection of
446 cell subpopulations. However, this specializes the Calu-3-ACE2 cells to infection with SARS-CoV-2
447 and is likely impacting infectability with other viruses. Similarly though, if a more highly
448 permissive version of Caki-1 cells was sought to study SARS-CoV-2 infection, selection of ACE2
449 cells may improve infection beyond 50%. We would, however, advise to keep this population as
450 is due to its broad susceptibility to a range of respiratory viruses.

451 Whilst Caki-1 are still a cancer cell line, and thus contain the mutations and caveats associated
452 with that fact, they have a well-characterized genome and expression patterns. Whilst they have
453 a knockout mutation in the CDKN2 gene and this should be kept in mind, they also boast a fully
454 receptive innate immune response, allowing this pathway to be interrogated
455 (https://www.cbioportal.org/, Accessed 8/10/2022, (36, 37)). This is also demonstrated by their
456 response to intracellular Poly I:C (a viral mimic), but not to LPS which is a bacterial stimulant of
457 immune cells, showing their response is specific and relevant to viral infections. Conversely, the
458 Vero E6 cells are defective in its production of interferon, but remains sensitive to the action of
459 interferon through ISGs, often making it a preferred cell line for the production of viral stocks,
460 with the caveat that attenuation is more likely (6).

461 With the emergence of new SARS-CoV-2 variants it has been found that in other cell lines, there
462 is a change in tropism and attachment / processing factor preference leading to a loss of infection
463 (38). Caki-1 cells are able to maintain equal levels of infection across all the VOCs tested (alpha,
464 delta, and omicron), without a change in phenotype, whereas Vero E6 cells lose their ability to
465 effectively support viral replication as the variants evolve. This decrease in permissibility of the
466 Vero E6 cells runs in parallel with the decrease in severe symptoms seen with the evolution of
467 the variants, with omicron causing the mildest disease of all the variants, likely attributed to a
468 change in cell tropism and / or temperature (39). As the Caki-1 cells can support infection of the
469 omicron variant, and it has been reported that omicron has moved away from TMPRSS2 mediated
470 entry (40), it could be assumed that entry into Caki-1 cells is less or not TMPRSS2 dependent. This
471 is reflected in the knockdown phenotypes (Figure 4B) with 25% relative infection still occurring
472 upon knockdown of TMPRSS2. This makes the Caki-1 cell line very valuable for future SARS-CoV-
473 2 research as they will be useful to study the host-virus interactions of variants evolved from
474 omicron.

475 The Caki-1 cell line also offers ideal growth characteristics for viral study and propagation. Whilst
476 being permissive to transfection Caki-1 cells have a doubling time of 36 hours (preventing
477 overgrowth), the cultures can pack tightly to form dense monolayers capable of supporting
478 widespread viral infection, and are robust enough to be able to maintain multi rounds of infection
479 without significant CPE development. Conversely, Vero E6, Calu-3, and Huh7 cells all develop CPE
480 after 24 hpi with SARS-CoV-2, restricting their use (7, 41). The slower growth of Caki-1 cells
481 compared to all other preferred cell lines, especially Vero E6 cells, also means that they are
482 suitable for producing stocks of slower growing viruses such as the common cold coronaviruses.
483 Here, we have also utilized Caki-1 cells to isolate clinical samples of SARS-CoV-2, specifically
484 omicron, a methodology which usually has been achieved on Vero E6 cells for all major virus
485 types. This negates the worry for mutation accumulation in the S1/S2 furin cleavage site that has
486 been observed in SARS-CoV-2 within a single passage in Vero E6 cells (7). The ability of Caki-1
487 cells to support robust infection with multiple respiratory viruses shows that this cell line can be
488 useful to study both coronaviruses and common cold viruses in direct comparison. The growth
489 properties of the cells furthermore improve high-throughput readouts and methods through
490 slower growth and overcrowding, reducing background fluorescence and changes to cell
491 properties in a dense cell layer.

492 The SARS-CoV-2 antibodies developed by MRC PPU Dundee form a useful toolset to quantify and
493 visualize viral proteins throughout the replication cycle as we have demonstrated here. We have
494 shown the localization of most viral proteins within Caki-1 cells, which agrees with the literature
495 for other cell lines localization and relevant SARS-CoV homologues (42, 43), and tagged proteins

496 in A549 cells (44). Contrast to the studies previously performed, here we can show how natural
497 expression of these proteins is characterized in cells where all other viral proteins and cellular
498 interaction partners are regulated through the viral infection. The staining and the advantage of
499 higher resolution techniques show the vast potential to study viral protein function through
500 localization. Particularly interesting will be the function of nuclear localization of NSP16 and
501 ORF9b. The many functions associated with proteins like N, ORF3B, NSP2, and NSP8 are indicated
502 through their broad distribution patterns within the cell. With these antibodies being raised in
503 sheep, they are ideal for pairing with other antibodies from other production animals for co-
504 localization studies. Here, we have used a variety of antibodies purified from different bleeds of
505 the production sheep as they were available to us. Indications are that later bleeds show less
506 background and more specific staining. It is clear that further optimization for some of the
507 staining protocols is warranted for some of the proteins of interest.

508 The multifaceted uses of Caki-1 cells in viral research are clear; they are easy to work with and
509 manipulate in the lab, they can support a range of viruses across multiple rounds of infection, and
510 in most cases outperform the commonly used cell line for each virus. They naturally highly
511 express a wide range of receptors, and possess an interferon response that can both produce and
512 respond, making them an ideal candidate for studying viral infections *in vitro*.

513 **Methods**

514 **Cells & Viruses**

515 Vero E6 (ATCC CRL-1586), Calu-3 (ATCC HTB-55), Huh-7 (JCRB, JCRB0403), HEp-2 (ATCC CCL-
516 23), and MDCK (ATCC CCL-34) cells were maintained as monolayer cultures in Dulbecco's
517 Modified Eagle's Medium (DMEM, Sigma), supplemented with 10% heat inactivated Fetal Bovine
518 Serum (FBS, Gibco), 1X Ultraglutamine-I (Lonza), and 1X Non-essential Amino Acids (NEAA,
519 Lonza) (complete DMEM). Calu-3 cells were supplemented with 1X Sodium Pyruvate (Sigma).
520 Hek-Blue IFN-α/β (InvivoGen) cells were maintained as monolayer cultures in complete DMEM
521 supplemented with 30 µg/ml of blasticidin (Gibco) and 100 µg/ml of Zeocin (Gibco). Caki-1 cells
522 (ATCC HTB-46) were maintained as monolayer cultures in Roswell Park Memorial Institute
523 medium (RPMI, Sigma), supplemented with 10% heat inactivated FBS (Gibco), 1X
524 Ultraglutamine-I (Lonza), and 1X NEAA (Lonza). Cells were maintained at 37°C in 5% CO_2.

525 Samples from confirmed COVID-19 patients were collected by trained healthcare professionals
526 using combined nose-and-throat swabbing. The samples were stored in virus transport medium
527 and sterile filtered through 0.1 µm filters prior to cultivation and isolation on Vero E6 cells.
528 Variant B.1.1.529 (o) was isolated on Caki-1 cells. Samples were anonymized by coding, compliant
529 with Tissue Governance for the South East Scotland Scottish 279 Academic Health Sciences
530 Collaboration Human Annotated BioResource (reference no. SR1452). Virus sequence was
531 confirmed by Nanopore sequencing according to the ARCTIC network protocol
532 (https://artic.network/ncov-2019), amplicon set V3, and validated against the patient isolate
533 sequence. SARS-CoV-2 variants utilized in this study are EDB-2 (B1.5 at the time, now B.1),
534 EDB-α-1 (B.1.1.7), EDB-δ-1 (B.1.617.2), and EDB-o-BA.1-1 (B.1.1.529, BA.1). Infectivity was
535 quantified by endpoint titration on Vero E6 cells, for all isolates apart from o (omicron), which
536 was titrated on Caki-1 cells. All infections in this study were performed using passage 2 from
537 isolation of each variant.

538 hCoV-229E-GFP (45) was propagated on Huh7 cells at 34°C with 5% CO_2 over 72 hours. Infectivity
539 was quantified by endpoint titration on Huh7 cells.

540 hRSV-A2-eGFP (46) (obtained from Juergen Schwarze, University of Edinburgh) was amplified on
541 HEp-2 cells over 72 hours. Infectivity was quantified by endpoint titration on HEp-2 cells.

542 MERS-CoV strain EMC (47) was propagated in VeroB4 cells. Infectivity was quantified by
543 endpoint titration on Huh7 cells as previously described (48).

544 Influenza A/Puerto Rico/8/1934 (H1N1) (IAV PR8) (49) was generated by reverse genetics as
545 described previously (50) and propagated on MDCK cells. Virus was titrated by plaque assay on
546 MDCK cells.

547 **Viral Growth Curves**

548 ***SARS-CoV-2***

549 Vero E6 and Caki-1 cells were seeded to confluence in a 24-well plate one day prior to inoculation
550 at differing MOIs for 1 h. At the indicated time point post infection, supernatant was lysed and
551 quantified as previously described (51). Briefly, the lysate was added to the reaction at 10% total
552 reaction volume and analyzed by RT-qPCR, using SYBR Green GoTaq 1-Step RT-qPCR (Promega)
553 with the SARS-CoV-2 CDC N3 primers (F – GGGAGCCTTGAATACACCAAAA, R –
554 TGTAGCACGATTGCAGCATTG) at 350 nM each to determine viral copy number according to the
555 manufacturer's instructions (annealing at 60°C) on a Stratagene MX3000p qPCR system. To
556 assess viral copy numbers, resulting Cts were analyzed against a standard curve of lysate with
557 known $TCID_{50}$/ml value as well as an RNA template.

558 ***hRSV and hCOV-229E***

559 HEp-2 (RSV), Huh7 (229E), and Caki-1 (both) cells were seeded to confluence in a black, clear
560 bottom 96-well plate one day prior to infection. After inoculation at differing MOIs for 1.5 h,
561 inoculum was removed and replication measured as a function of GFP fluorescence from 6 hpi to
562 72 hpi in 2-hour intervals (BMG Clariostar; excitation: 470-15, dichroic: 492.5, emission: 515-15,
563 bottom optic). Slopes of the linear phase of replication were calculated then normalized to
564 uninfected cells (slope = 1) and the average slope calculated.

565 ***MERS-CoV***

566 Huh7 and Caki-1 cells were seeded to confluence one day prior to infection. After inoculation at
567 differing MOIs for 2 h inoculum was removed and cells were washed three times with PBS. At
568 indicated time points post infection, supernatant was lysed and quantified as previously
569 described. Virus titers were determined by endpoint titration on Huh7 cells inoculated with serial
570 dilution and $TCID_{50}$/ml was visualized using Crystal Violet 72 hpi and calculated by the
571 Spearman–Kärber algorithm.

572 ***IAV***

573 MDCK and Caki-1 cells were seeded to confluence one day prior to infection. After inoculation at
574 MOI=0.01 for 1 h, inoculum was replaced with serum free medium containing 1 µg/ml tosyl
575 phenylalanyl chloromethyl ketone (TPCK)-treated trypsin (Sigma) and 0.14% BSA (w/v) (Sigma).
576 Infected cells were incubated at 37°C for the duration of the experiment and supernatant samples
577 harvested at indicated time points. Virus titers were determined by plaque titration using ten-fold
578 serial dilutions of virus stocks. Confluent MDCK cells in 6 well plates were inoculated with virus
579 stock for 1 h, then an overlay (mixture of equal volume of DMEM and 2.4% Avicel (Sigma-Aldrich,
580 UK) supplemented with 1 µg/ml TPCK-treated trypsin and 0.14% BSA fraction V) was put onto
581 the wells. After 48 hpi, cells were fixed using 3.5% formaldehyde and stained with 0.1% crystal

582 violet. Virus titers were calculated by plaque count*dilution factor/(volume of inoculum) and
583 expressed as PFU/ml.

584 **Fluorescent Activated Cell Sorting (FACS) of Calu-3 cells**

585 Calu-3 cells were enriched for high ACE2 expression (Calu-3-ACE2) by FACS using a BD
586 Biosciences FACSAria III Cell Sorter. Cells were detached from a T75 using Gentle Cell Dissociation
587 Reagent (Stemcell Technologies) and recovered in DMEM prior to staining. Recombinant
588 Anti-ACE2 antibody (Abcam, ab272500) was used at 1:500 before staining with Goat anti-Rabbit
589 IgG (H+L) AF647 (Invitrogen, A-21244) at 1:2000. The top 0.1% of cells expressing ACE2 were
590 collected and cultured in conditioned media to recover and expand.

591 **Flow Cytometry**

592 Vero E6, Caki-1, Calu-3, and Calu-3-ACE2 cells were seeded one day prior to inoculation with
593 SARS-CoV-2-EDB-2 at differing MOIs of 10, 1 and 0.1 for 1 h. At the indicated timepoints, the cells
594 were detached from the well using TrypLE Express Enzyme (Gibco) prior to fixation with 4%
595 formaldehyde. The cells were permeabilized using 0.1% Triton-X-100. Using standard
596 immunocytochemistry techniques, primary antibody targeting SARS-CoV-2 N protein (DA114 4th
597 bleed, MRC PPU Dundee, generated as described in (16)) was used at 1:200 (Table 1) before
598 staining with Donkey anti-Sheep AF488 Secondary Antibody (Invitrogen, A-11015) at 1:2000.
599 The cells were analyzed using a B530/30-A filter on a BD Biosciences LSRFortessa X-20 Cell
600 Analyzer.

601 *Table 1: Antibodies targeting SARS-CoV-2 generated by the MRC PPU and respective concentrations used.*

TARGET	ID	BLEED	STOCK CONC. (MG/ML)	IF	FLOW
				Dil. / conc. (µg/ml)	
NSP1	DA103	1st	0.38	1:200 / 1.9	
NSP2	DA105	1st	0.15	1:200 / 0.75	
NSP3 (743-1072)	DA126	1st	0.13	1:200 / 0.65	
NSP5	DA118	1st	0.35	1:200 / 1.75	
NSP7	DA093	2nd	0.23	1:200 / 1.15	
NSP8	DA110	1st	0.44	1:200 / 2.2	
NSP9	DA094	2nd	0.33	1:200 / 1.65	
NSP10	DA091	2nd	0.27	1:200 / 1.35	
NSP11/12	DA119	1st	0.2	1:200 / 1	
NSP13	DA111	1st	0.29	1:200 / 1.45	
NSP14	DA112	1st	0.22	1:200 / 1.1	
NSP15	DA120	1st	0.14	1:200 / 0.7	
NSP16	DA113	1st	0.36	1:200 / 1.8	
S (ORF2)	DA123	5th	1.05	1:200 / 5.25	
S (RBD, ORF2)	DA125	5th	0.18	1:200 / 0.9	
ORF3A	DA102	1st	0.2	1:200 / 1	

ORF3B	DA100	2nd	0.24	1:200 / 1.2	
E (ORF4)	DA108	1st	0.12	1:200 / 0.6	
M (ORF5)	DA107	1st	0.15	1:200 / 0.75	
ORF6	DA087	2nd	0.14	1:200 / 0.7	
ORF7A	DA124	1st	0.32	1:200 / 1.6	
ORF7B	DA092	2nd	0.17	1:200 / 0.85	
ORF8	DA088	2nd	0.12	1:200 / 0.6	
N (ORF9)	DA114	1st	0.32	1:200 / 1.6	
N (ORF9)	DA114	4th	0.32		1:200 / 1.6
ORF9B	DA089	2nd	0.28	1:200 / 1.4	
ORF9C	DA101	2nd	0.35	1:200 / 1.75	
ORF10	DA090	2nd	0.21	1:200 / 1.05	

Confocal Imaging

Caki-1 cells were seeded in clear-bottom Lumox plates (Sarstedt) one day prior to infection with EDB-2 at MOI = 1. At 16 hpi the cells were fixed with 4% formaldehyde and permeabilized using 0.1% Triton-X-100. Using standard immunocytochemistry techniques, primary antibodies targeting SARS-CoV-2 proteins were used at indicated dilutions / concentrations (Table 1, MRC PPU Dundee) before staining with Donkey anti-Sheep AF488 Secondary Antibody (Invitrogen) at 1:2000, DAPI (Invitrogen, A-11015) at 0.2 µg/ml, and Alexa Fluor™ 594 Phalloidin (Invitrogen) at 1:5,000. The cells were analyzed on a Zeiss LSM 880 Airyscan microscope acquiring z-stack images with a set 0.5 µm imaging interval in the z-direction. Imaging properties were set for an uninfected, stained control sample for each antibody. Images were processed using Fiji (ImageJ) to generate maximum projection images, merge, and montage.

Receptor Quantification

RNA was extracted from Caki-1 cells using the RNeasy (Qiagen) kit according to the manufacturer's instructions. RNA was quantified by Nanodrop and Qubit (ThermoFisher). RT-qPCR reactions using the GoTaq 1-Step RT-qPCR kit (Promega) were set-up to 10 µl final reaction volumes according to the manufacturer's instructions containing 250 nM of each receptors primer pairs and 10 ng of RNA. The RT-qPCR was run on a Mx3000P (Agilent) using an annealing temperature of 60°C and analyzed against a standard curve of Mitochondrial 18S ribosomal RNA (RRN18S) before being normalized to the RRN18 value. Primers used were ACE2 (fwd: TTCCACTCTCATTTGAGCCTG, rev: GCCGGAGATAGGAGTGGA), TMPRSS2 (fwd: AGGGAAGACCTCAGAAGTGC, rev: CACAGATCATGGCTGGTGTG), NRP1 (fwd: TCCTCATCGGGCATTCTCTC, rev: TCTGAGACACTGCTCTGCAA, ANPEP (fwd: TTCAACATCACGCTTATCCACC, rev: AGTCGAACTCACTGACAATGAAG), DPP4 (fwd: TACAAAAGTGACATGCCTCAGTT, rev: TGTGTAGAGTATAGAGGGGCAGA), and RRN18S (fwd: AGAAACGGCTACCACATCCA, rev: CACCAGACTTGCCCTCCA).

628 **Receptor siRNA knockdown**

629 siRNA (Dharmacon – Table 2) and Dharmafect 1 (Horizon) were combined in OptiMEM (Gibco)
630 to achieve a final concentration of 20 nM and 0.1% respectively. Transfection complexes were
631 incubated for 20 minutes at room temperature before the addition of 20,000 cells per 96-well. At
632 72 h post transfection, cells were infected with EDB-2 at MOI = 0.1. At 24 and 48 hpi, supernatant
633 was harvested, lysed, and quantified as as previously described (51). Relative quantities were
634 normalized to the Non-targeting control (#1).

635 *Table 2: Dharmacon siRNA sequences used in this study.*

Gene	siRNA sequence (sense)
ACE2	GAACAUACCUUUGAAGAGA, GCACAAAGGUGACAAUGGA, GGAGGUGGAUGGUCUUUAA, GAGAGGAGACUAUGAAGUA
TMPRSS2	GCAAUGUCGAUAUCUAUAA, GCUAUUGGACCUUACUAUG, ACGGGAAUGUGAUGGUAUU, CGGACUGGAUUUAUCGACA
NRP1	GACCAGGACUACAGGGUUA, GAGGACGGCAUGAGACUUA, CCAGGUGUAUUCCGAACUU, GCCGAGGACCCGAAGGUUA
Cathepsin B	GGAUCACUGUGGAAUCGAA, GGAACUUCUGGACAAGAAA, GGAUGAGCUGGUCAACUAU, GGCACAACUUCUACAACGU
Cathepsin L	CAGCUACUCUAACAUUUGA, UCCAGUAUGUUCAGGAUAA, GGAGAAACCAUUGUGGAAU, CAGAUUAUACGGCAUGAAU
Non-Targeting (control #1)	UAGCGACUAAACACAUCAA, UAAGGCUAUGAAGAGAUAC, AUGUAUUGGCCUGUAUUAG, AUGAACGUGAAUUGCUCAA
SARs2 N protein	AGAACAAACCCAAGGAAAUUU

636

637 **Cell Viability Assay**

638 Caki-1 cells were seeded onto a black-sided, clear-bottomed 96-well plates after reverse
639 transfection with siRNA (20 nM, as described above) and incubated for 72 h. CellTiter-Blue
640 (Promega, G8080) reagent was added to each well at a 1:10 ratio. Following 3 hours of incubation
641 at 37°C, fluorescence as a result of metabolic activity was measured using the BMG Clariostar
642 plate reader (excitation: 545-20, emission: 600-40, 30 flashes/well, bottom optic) and
643 fluorescence intensity was compared between the untreated and the drug treated cells to
644 calculate a percentage viability.

645 **HEK-Blue Interferon Assay**

646 Caki-1 cells were seeded in a 12-well plate and stimulated by either reverse transfecting with
647 Poly I:C (Enzo) using Dharmafect 1 (working concentration of 0.1%), or with media containing
648 Poly I:C (Enzo) or LPS (Sigma) at the indicated concentrations. At 24 hours post treatment,
649 supernatant was harvested and 20 µl added to confluent HEK-Blue IFNα/β cells for 24 h. 20 µl of
650 induced HEK-Blue cell supernatant was added to a corresponding plate with 180 µL of
651 Quanti-Blue substrate in each well. After 3 h incubation SEAP levels were detected using the
652 Clariostar (BMG) at 640 nm.

653 **Figure Legends**

654 **Figure 1: Time course assays in coronaviruses comparing the most commonly used cell**
655 **line with Caki-1.** For all graphs: circle points = MOI 10, square points = MOI 1, triangle points =
656 MOI 0.1, diamond points = MOI 0.01, and the darker the color the higher the MOI, error bars
657 indicate +/- SEM. [A] Time course infection of SARS-CoV-2 variants on Vero E6 and Caki-1 cells,
658 biological n=3x3. Measured through RT-qPCR for the SARS-CoV-2 N gene in the supernatant,
659 samples taken at 0, 6, 16, 24, 48, 72, 96 and 120 hpi at MOIs of 10, 1 and 0.1. [B] Time course
660 infection of MERS-CoV on Huh-7 and Caki-1 cells, biological n=3x3, measured through TCID50 on
661 Huh-7 cells. Samples taken at 24h intervals until 96hpi. [C] GFP time course of infection for
662 hCoV-229E on Huh-7 and Caki-1 cells, measured from 0 hpi to 78 hpi in 6 h intervals, with
663 fluorescence as a proxy for viral replication, biological n=3x3. [D] Fluorescence-activated cell
664 sorting to determine the percentage of infected SARS-CoV-2 cells in Vero E6, Caki-1, Calu-3 and
665 Calu-3-ACE2 cells. Vero E6 and Caki-1 cells were fixed at 17 hpi, stained for intracellular SARS-
666 CoV-2 N protein and sorted for fluorescent cells, biological n=3x3. The same was conducted for
667 Calu-3 and Calu-3-ACE2 cells at 24 hpi and 48 hpi, biological n=3x3.

668 **Figure 2: Confocal analysis of Caki-1 cells showing localization and size of SARS-CoV-2 orf**
669 **proteins.** [A] SARS-CoV-2 genome illustrating the proteins translated by the viral genome and
670 their relative sizes. [B] Immunocytochemsitry staining showing infected and uninfected Caki-1
671 cells stained for SARS-CoV-2 open reading frame proteins. The protein of interest (POI) is
672 indicated in green, the DAPI indicating DNA and RNA in blue, and actin in red. Scale bar represents
673 20 μM.

674 **Figure 3: Confocal analysis of Caki-1 cells showing localisation and size of SARS-CoV-2 NSP**
675 **proteins.** Immunocytochemsitry staining showing infected and uninfected Caki-1 cells stained
676 for SARS-CoV-2 non-structural proteins. The POI is indicated in green, the DAPI indicating DNA
677 and RNA in blue, and actin in red. Scale bar represents 20 μm.

678 **Figure 4: Characterizing Caki-1 cells in the context of respiratory virus infection with**
679 **receptor and interferon competence profiling.** [A] Violin plot showing the entry factors for the
680 human coronaviruses; ACE2, TMPRSS2, NRP1, ANPEP, and DPP4 checked for mRNA expression
681 in Caki-1 cells, relative to expression of the housekeeping gene RRN18S. Biological n=3x2. [B]
682 (left) Relative replication of SARS-CoV-2 after knockdown of the entry factors in Caki-1 cells
683 relative to the scrambled siRNA non-targeting at 24 hpi, all knockdowns are significant to a
684 p-value < 0.0001, biological n=12x3, error bars representing +/-SEM. (right) Cell viability after
685 knockdown of SARS-CoV-2 entry factors for 72 h, dotted line indicates the cut-off for 80% relative
686 cell viability, biological nx3, error bars represent +/-SEM. [C] Box and whiskers plot indicating

687 the interferon α/β stimulation of Caki-1 cells after treatment with LPS and Poly I:C, TF indicates
688 transfection into the cell. All overlay treatments are non-significant, but transfection of Poly I:C at
689 1 μg/ml and 10 μg/ml were significant to 0.0001 and 0.001 respectively. [D] Time course of
690 infection in Caki-1 cells (dark red filled squares) compared to MDCK (light red hollow squares)
691 cells for IAV PR8, time points taken at 0, 12, 24 and 48 hpi and plaqued on MDCK cells to
692 determine pfu/ml, biological n=3, error bars representing +/-SEM. [E] RSV-A2-GFP replication
693 in HEp-2 cells (turquoise hollow squares) compared to Caki-1 cells (dark blue filled squares)
694 every 6 hpi up to 78 hpi monitored by fluorescence of GFP. Biological n=3x3, error bars represent
695 +/-SEM.

696

697

698 **References**

699 1. de Groot RJB, S. C.; Baric, R.; Enjuanes, L.; Gorbalenya, A. E.; Holmes, K. V.; Perlman, S.; Poon,
700 L.; Rottier, P. J. M.; Talbot, P. J.; Woo, P. C. Y.; Ziebuhr, J. 2011. Virus Taxonomy: Ninth Report
701 of the International Committee on Taxonomy of Viruses, p 806-828. *In* King AMQA, M. J.;
702 Castens, E. B.; Lefkowitz, E. J. (ed) doi:https://doi.org/10.1016/B978-0-12-384684-6.00068-9.
703 Elsevier Academic Press, London.
704 2. Peiris JS, Lai ST, Poon LL, Guan Y, Yam LY, Lim W, Nicholls J, Yee WK, Yan WW, Cheung MT,
705 Cheng VC, Chan KH, Tsang DN, Yung RW, Ng TK, Yuen KY, group Ss. 2003. Coronavirus as a
706 possible cause of severe acute respiratory syndrome. Lancet 361:1319-25.
707 3. Zaki AM, van Boheemen S, Bestebroer TM, Osterhaus AD, Fouchier RA. 2012. Isolation of a
708 novel coronavirus from a man with pneumonia in Saudi Arabia. N Engl J Med 367:1814-20.
709 4. Wu P, Hao X, Lau EHY, Wong JY, Leung KSM, Wu JT, Cowling BJ, Leung GM. 2020. Real-time
710 tentative assessment of the epidemiological characteristics of novel coronavirus infections in
711 Wuhan, China, as at 22 January 2020. Euro Surveill 25.
712 5. Pommerenke C, Rand U, Uphoff CC, Nagel S, Zaborski M, Hauer V, Kaufmann M, Meyer C,
713 Denkmann SA, Riese P, Eschke K, Kim Y, Safranko ZM, Kurolt IC, Markotic A, Cicin-Sain L,
714 Steenpass L. 2021. Identification of cell lines CL-14, CL-40 and CAL-51 as suitable models for
715 SARS-CoV-2 infection studies. PLoS One 16:e0255622.
716 6. Desmyter J, Melnick JL, Rawls WE. 1968. Defectiveness of interferon production and of rubella
717 virus interference in a line of African green monkey kidney cells (Vero). J Virol 2:955-61.
718 7. Ogando NS, Dalebout TJ, Zevenhoven-Dobbe JC, Limpens RWAL, van der Meer Y, Caly L, Druce
719 J, de Vries JJC, Kikkert M, Bárcena M, Sidorov I, Snijder EJ. 2020. SARS-coronavirus-2
720 replication in Vero E6 cells: replication kinetics, rapid adaptation and cytopathology. J Gen
721 Virol 101:925-940.
722 8. Chu H, Chan JF, Yuen TT, Shuai H, Yuan S, Wang Y, Hu B, Yip CC, Tsang JO, Huang X, Chai Y,
723 Yang D, Hou Y, Chik KK, Zhang X, Fung AY, Tsoi HW, Cai JP, Chan WM, Ip JD, Chu AW, Zhou J,
724 Lung DC, Kok KH, To KK, Tsang OT, Chan KH, Yuen KY. 2020. Comparative tropism, replication
725 kinetics, and cell damage profiling of SARS-CoV-2 and SARS-CoV with implications for clinical
726 manifestations, transmissibility, and laboratory studies of COVID-19: an observational study.
727 Lancet Microbe 1:e14-e23.
728 9. Wei J, Alfajaro MM, DeWeirdt PC, Hanna RE, Lu-Culligan WJ, Cai WL, Strine MS, Zhang SM,
729 Graziano VR, Schmitz CO, Chen JS, Mankowski MC, Filler RB, Ravindra NG, Gasque V, de Miguel
730 FJ, Patil A, Chen H, Oguntuyo KY, Abriola L, Surovtseva YV, Orchard RC, Lee B, Lindenbach BD,
731 Politi K, van Dijk D, Kadoch C, Simon MD, Yan Q, Doench JG, Wilen CB. 2021. Genome-wide
732 CRISPR Screens Reveal Host Factors Critical for SARS-CoV-2 Infection. Cell 184:76-91 e13.
733 10. Zhu Y, Feng F, Hu G, Wang Y, Yu Y, Zhu Y, Xu W, Cai X, Sun Z, Han W, Ye R, Qu D, Ding Q, Huang
734 X, Chen H, Xu W, Xie Y, Cai Q, Yuan Z, Zhang R. 2021. A genome-wide CRISPR screen identifies
735 host factors that regulate SARS-CoV-2 entry. Nat Commun 12:961.
736 11. Daniloski Z, Jordan TX, Wessels HH, Hoagland DA, Kasela S, Legut M, Maniatis S, Mimitou EP,
737 Lu L, Geller E, Danziger O, Rosenberg BR, Phatnani H, Smibert P, Lappalainen T, tenOever BR,
738 Sanjana NE. 2021. Identification of Required Host Factors for SARS-CoV-2 Infection in Human
739 Cells. Cell 184:92-105 e16.
740 12. Schneider WM, Luna JM, Hoffmann HH, Sanchez-Rivera FJ, Leal AA, Ashbrook AW, Le Pen J,
741 Ricardo-Lax I, Michailidis E, Peace A, Stenzel AF, Lowe SW, MacDonald MR, Rice CM, Poirier
742 JT. 2021. Genome-Scale Identification of SARS-CoV-2 and Pan-coronavirus Host Factor
743 Networks. Cell 184:120-132 e14.
744 13. Wang L, Fan X, Bonenfant G, Cui D, Hossain J, Jiang N, Larson G, Currier M, Liddell J, Wilson M,
745 Tamin A, Harcourt J, Ciomperlik-Patton J, Pang H, Dybdahl-Sissoko N, Campagnoli R, Shi PY,
746 Barnes J, Thornburg NJ, Wentworth DE, Zhou B. 2021. Susceptibility to SARS-CoV-2 of Cell
747 Lines and Substrates Commonly Used to Diagnose and Isolate Influenza and Other Viruses.
748 Emerg Infect Dis 27:1380-1392.

749 14. Wang G, Barrett JW, Stanford M, Werden SJ, Johnston JB, Gao X, Sun M, Cheng JQ, McFadden
750 G. 2006. Infection of human cancer cells with myxoma virus requires Akt activation via
751 interaction with a viral ankyrin-repeat host range factor. Proc Natl Acad Sci U S A 103:4640-5.
752 15. Lee HL, Essani K. 2010. Differential susceptibility of human cancer cell lines to wild-type
753 tanapoxvirus infection. Open Virol J 4:1-6.
754 16. Rihn SJ, Merits A, Bakshi S, Turnbull ML, Wickenhagen A, Alexander AJT, Baillie C, Brennan B,
755 Brown F, Brunker K, Bryden SR, Burness KA, Carmichael S, Cole SJ, Cowton VM, Davies P, Davis
756 C, De Lorenzo G, Donald CL, Dorward M, Dunlop JI, Elliott M, Fares M, da Silva Filipe A, Freitas
757 JR, Furnon W, Gestuveo RJ, Geyer A, Giesel D, Goldfarb DM, Goodman N, Gunson R, Hastie CJ,
758 Herder V, Hughes J, Johnson C, Johnson N, Kohl A, Kerr K, Leech H, Lello LS, Li K, Lieber G, Liu
759 X, Lingala R, Loney C, Mair D, McElwee MJ, McFarlane S, Nichols J, et al. 2021. A plasmid DNA-
760 launched SARS-CoV-2 reverse genetics system and coronavirus toolkit for COVID-19 research.
761 PLoS Biol 19:e3001091.
762 17. McBride CE, Li J, Machamer CE. 2007. The cytoplasmic tail of the severe acute respiratory
763 syndrome coronavirus spike protein contains a novel endoplasmic reticulum retrieval signal
764 that binds COPI and promotes interaction with membrane protein. J Virol 81:2418-28.
765 18. Ujike M, Huang C, Shirato K, Makino S, Taguchi F. 2016. The contribution of the cytoplasmic
766 retrieval signal of severe acute respiratory syndrome coronavirus to intracellular
767 accumulation of S proteins and incorporation of S protein into virus-like particles. J Gen Virol
768 97:1853-1864.
769 19. Lu W, Zheng BJ, Xu K, Schwarz W, Du L, Wong CK, Chen J, Duan S, Deubel V, Sun B. 2006.
770 Severe acute respiratory syndrome-associated coronavirus 3a protein forms an ion channel
771 and modulates virus release. Proc Natl Acad Sci U S A 103:12540-5.
772 20. Zhang Y, Sun H, Pei R, Mao B, Zhao Z, Li H, Lin Y, Lu K. 2021. The SARS-CoV-2 protein ORF3a
773 inhibits fusion of autophagosomes with lysosomes. Cell Discov 7:31.
774 21. Freundt EC, Yu L, Park E, Lenardo MJ, Xu XN. 2009. Molecular determinants for subcellular
775 localization of the severe acute respiratory syndrome coronavirus open reading frame 3b
776 protein. J Virol 83:6631-40.
777 22. Konno Y, Kimura I, Uriu K, Fukushi M, Irie T, Koyanagi Y, Sauter D, Gifford RJ, Nakagawa S, Sato
778 K, Consortium U-C. 2020. SARS-CoV-2 ORF3b Is a Potent Interferon Antagonist Whose Activity
779 Is Increased by a Naturally Occurring Elongation Variant. Cell Rep 32:108185.
780 23. Schaecher SR, Mackenzie JM, Pekosz A. 2007. The ORF7b protein of severe acute respiratory
781 syndrome coronavirus (SARS-CoV) is expressed in virus-infected cells and incorporated into
782 SARS-CoV particles. J Virol 81:718-31.
783 24. Matsuoka K, Imahashi N, Ohno M, Ode H, Nakata Y, Kubota M, Sugimoto A, Imahashi M,
784 Yokomaku Y, Iwatani Y. 2022. SARS-CoV-2 accessory protein ORF8 is secreted extracellularly
785 as a glycoprotein homodimer. J Biol Chem 298:101724.
786 25. Boson B, Legros V, Zhou B, Siret E, Mathieu C, Cosset FL, Lavillette D, Denolly S. 2021. The
787 SARS-CoV-2 envelope and membrane proteins modulate maturation and retention of the
788 spike protein, allowing assembly of virus-like particles. J Biol Chem 296:100111.
789 26. Lee HK, Lee BH, Seok SH, Baek MW, Lee HY, Kim DJ, Na YR, Noh KJ, Park SH, Kumar DN, Kariwa
790 H, Nakauchi M, Heo SJ, Park JH. 2010. Production of specific antibodies against SARS-
791 coronavirus nucleocapsid protein without cross reactivity with human coronaviruses 229E and
792 OC43. J Vet Sci 11:165-7.
793 27. Gordon DE, Jang GM, Bouhaddou M, Xu J, Obernier K, White KM, O'Meara MJ, Rezelj VV, Guo
794 JZ, Swaney DL, Tummino TA, Hüttenhain R, Kaake RM, Richards AL, Tutuncuoglu B, Foussard
795 H, Batra J, Haas K, Modak M, Kim M, Haas P, Polacco BJ, Braberg H, Fabius JM, Eckhardt M,
796 Soucheray M, Bennett MJ, Cakir M, McGregor MJ, Li Q, Meyer B, Roesch F, Vallet T, Mac Kain
797 A, Miorin L, Moreno E, Naing ZZC, Zhou Y, Peng S, Shi Y, Zhang Z, Shen W, Kirby IT, Melnyk JE,
798 Chorba JS, Lou K, Dai SA, Barrio-Hernandez I, Memon D, Hernandez-Armenta C, et al. 2020. A

799 SARS-CoV-2 protein interaction map reveals targets for drug repurposing. Nature 583:459-
800 468.
801 28. Shi CS, Qi HY, Boularan C, Huang NN, Abu-Asab M, Shelhamer JH, Kehrl JH. 2014. SARS-
802 coronavirus open reading frame-9b suppresses innate immunity by targeting mitochondria
803 and the MAVS/TRAF3/TRAF6 signalosome. J Immunol 193:3080-9.
804 29. Cornillez-Ty CT, Liao L, Yates JR, Kuhn P, Buchmeier MJ. 2009. Severe acute respiratory
805 syndrome coronavirus nonstructural protein 2 interacts with a host protein complex involved
806 in mitochondrial biogenesis and intracellular signaling. J Virol 83:10314-8.
807 30. Lei J, Kusov Y, Hilgenfeld R. 2018. Nsp3 of coronaviruses: Structures and functions of a large
808 multi-domain protein. Antiviral Res 149:58-74.
809 31. Wang Q, Wu J, Wang H, Gao Y, Liu Q, Mu A, Ji W, Yan L, Zhu Y, Zhu C, Fang X, Yang X, Huang Y,
810 Gao H, Liu F, Ge J, Sun Q, Xu W, Liu Z, Yang H, Lou Z, Jiang B, Guddat LW, Gong P, Rao Z. 2020.
811 Structural Basis for RNA Replication by the SARS-CoV-2 Polymerase. Cell 182:417-428.e13.
812 32. Lin S, Chen H, Chen Z, Yang F, Ye F, Zheng Y, Yang J, Lin X, Sun H, Wang L, Wen A, Dong H, Xiao
813 Q, Deng D, Cao Y, Lu G. 2021. Crystal structure of SARS-CoV-2 nsp10 bound to nsp14-ExoN
814 domain reveals an exoribonuclease with both structural and functional integrity. Nucleic Acids
815 Res 49:5382-5392.
816 33. Yadav R, Chaudhary JK, Jain N, Chaudhary PK, Khanra S, Dhamija P, Sharma A, Kumar A, Handu
817 S. 2021. Role of Structural and Non-Structural Proteins and Therapeutic Targets of SARS-CoV-
818 2 for COVID-19. Cells 10.
819 34. Zillessen P, Celner J, Kretschmann A, Pfeifer A, Racke K, Mayer P. 2016. Metabolic role of
820 dipeptidyl peptidase 4 (DPP4) in primary human (pre)adipocytes. Sci Rep 6:23074.
821 35. Hasan MR, Ahmad MN, Dargham SR, Zayed H, Al Hashemi A, Ngwabi N, Perez Lopez A, Dobson
822 S, Abu Raddad LJ, Tang P. 2021. Nasopharyngeal Expression of Angiotensin-Converting
823 Enzyme 2 and Transmembrane Serine Protease 2 in Children within SARS-CoV-2-Infected
824 Family Clusters. Microbiol Spectr 9:e0078321.
825 36. Gao J, Aksoy BA, Dogrusoz U, Dresdner G, Gross B, Sumer SO, Sun Y, Jacobsen A, Sinha R,
826 Larsson E, Cerami E, Sander C, Schultz N. 2013. Integrative analysis of complex cancer
827 genomics and clinical profiles using the cBioPortal. Sci Signal 6:pl1.
828 37. Cerami E, Gao J, Dogrusoz U, Gross BE, Sumer SO, Aksoy BA, Jacobsen A, Byrne CJ, Heuer ML,
829 Larsson E, Antipin Y, Reva B, Goldberg AP, Sander C, Schultz N. 2012. The cBio cancer genomics
830 portal: an open platform for exploring multidimensional cancer genomics data. Cancer Discov
831 2:401-4.
832 38. Mautner L, Hoyos M, Dangel A, Berger C, Ehrhardt A, Baiker A. 2022. Replication kinetics and
833 infectivity of SARS-CoV-2 variants of concern in common cell culture models. Virol J 19:76.
834 39. Schulze H, Bayer W. 2022. Changes in Symptoms Experienced by SARS-CoV-2-Infected
835 Individuals – From the First Wave to the Omicron Variant. Frontiers in Virology 2.
836 40. Meng B, Abdullahi A, Ferreira I, Goonawardane N, Saito A, Kimura I, Yamasoba D, Gerber PP,
837 Fatihi S, Rathore S, Zepeda SK, Papa G, Kemp SA, Ikeda T, Toyoda M, Tan TS, Kuramochi J,
838 Mitsunaga S, Ueno T, Shirakawa K, Takaori-Kondo A, Brevini T, Mallery DL, Charles OJ,
839 Collaboration C-NBC-, Genotype to Phenotype Japan C, Ecuador CC, Bowen JE, Joshi A, Walls
840 AC, Jackson L, Martin D, Smith KGC, Bradley J, Briggs JAG, Choi J, Madissoon E, Meyer KB,
841 Mlcochova P, Ceron-Gutierrez L, Doffinger R, Teichmann SA, Fisher AJ, Pizzuto MS, de Marco
842 A, Corti D, Hosmillo M, Lee JH, James LC, Thukral L, et al. 2022. Altered TMPRSS2 usage by
843 SARS-CoV-2 Omicron impacts infectivity and fusogenicity. Nature 603:706-714.
844 41. Tseng CT, Tseng J, Perrone L, Worthy M, Popov V, Peters CJ. 2005. Apical entry and release of
845 severe acute respiratory syndrome-associated coronavirus in polarized Calu-3 lung epithelial
846 cells. J Virol 79:9470-9.
847 42. You J, Dove BK, Enjuanes L, DeDiego ML, Alvarez E, Howell G, Heinen P, Zambon M, Hiscox JA.
848 2005. Subcellular localization of the severe acute respiratory syndrome coronavirus
849 nucleocapsid protein. J Gen Virol 86:3303-3310.

850 43. Yuan X, Li J, Shan Y, Yang Z, Zhao Z, Chen B, Yao Z, Dong B, Wang S, Chen J, Cong Y. 2005.
851 Subcellular localization and membrane association of SARS-CoV 3a protein. Virus Res 109:191-
852 202.
853 44. Miserey-Lenkei S, Trajkovic K, D'Ambrosio JM, Patel AJ, Čopič A, Mathur P, Schauer K, Goud B,
854 Albanèse V, Gautier R, Subra M, Kovacs D, Barelli H, Antonny B. 2021. A comprehensive library
855 of fluorescent constructs of SARS-CoV-2 proteins and their initial characterisation in different
856 cell types. Biol Cell 113:311-328.
857 45. Cervantes-Barragan L, Zust R, Maier R, Sierro S, Janda J, Levy F, Speiser D, Romero P, Rohrlich
858 PS, Ludewig B, Thiel V. 2010. Dendritic cell-specific antigen delivery by coronavirus vaccine
859 vectors induces long-lasting protective antiviral and antitumor immunity. mBio 1.
860 46. Hallak LK, Collins PL, Knudson W, Peeples ME. 2000. Iduronic acid-containing
861 glycosaminoglycans on target cells are required for efficient respiratory syncytial virus
862 infection. Virology 271:264-75.
863 47. Kindler E, Jonsdottir HR, Muth D, Hamming OJ, Hartmann R, Rodriguez R, Geffers R, Fouchier
864 RA, Drosten C, Muller MA, Dijkman R, Thiel V. 2013. Efficient replication of the novel human
865 betacoronavirus EMC on primary human epithelium highlights its zoonotic potential. mBio
866 4:e00611-12.
867 48. Kratzel A, Kelly JN, V'Kovski P, Portmann J, Bruggemann Y, Todt D, Ebert N, Shrestha N, Plattet
868 P, Staab-Weijnitz CA, von Brunn A, Steinmann E, Dijkman R, Zimmer G, Pfaender S, Thiel V.
869 2021. A genome-wide CRISPR screen identifies interactors of the autophagy pathway as
870 conserved coronavirus targets. PLoS Biol 19:e3001490.
871 49. de Wit E, Spronken MI, Bestebroer TM, Rimmelzwaan GF, Osterhaus AD, Fouchier RA. 2004.
872 Efficient generation and growth of influenza virus A/PR/8/34 from eight cDNA fragments.
873 Virus Res 103:155-61.
874 50. Hutchinson EC, Curran MD, Read EK, Gog JR, Digard P. 2008. Mutational analysis of cis-acting
875 RNA signals in segment 7 of influenza A virus. J Virol 82:11869-79.
876 51. Craig N, Fletcher SL, Daniels A, Newman C, O'Shea M, Tan WS, Warr A, Tait-Burkard C. 2022.
877 Direct Lysis RT-qPCR of SARS-CoV-2 in Cell Culture Supernatant Allows for Fast and Accurate
878 Quantification. Viruses 14.

879

880 **Figure 1**

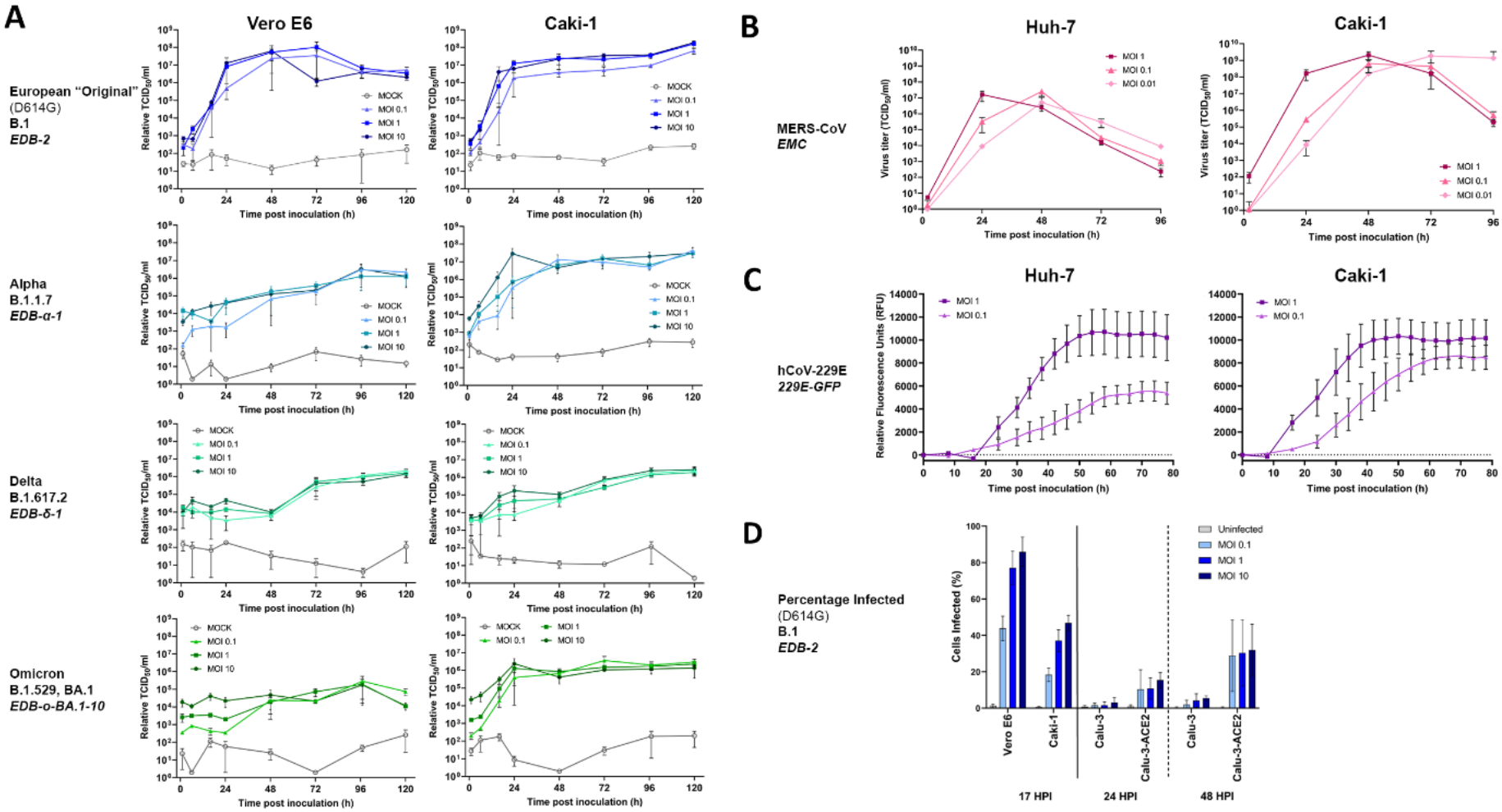

881

882 **Figure 2**

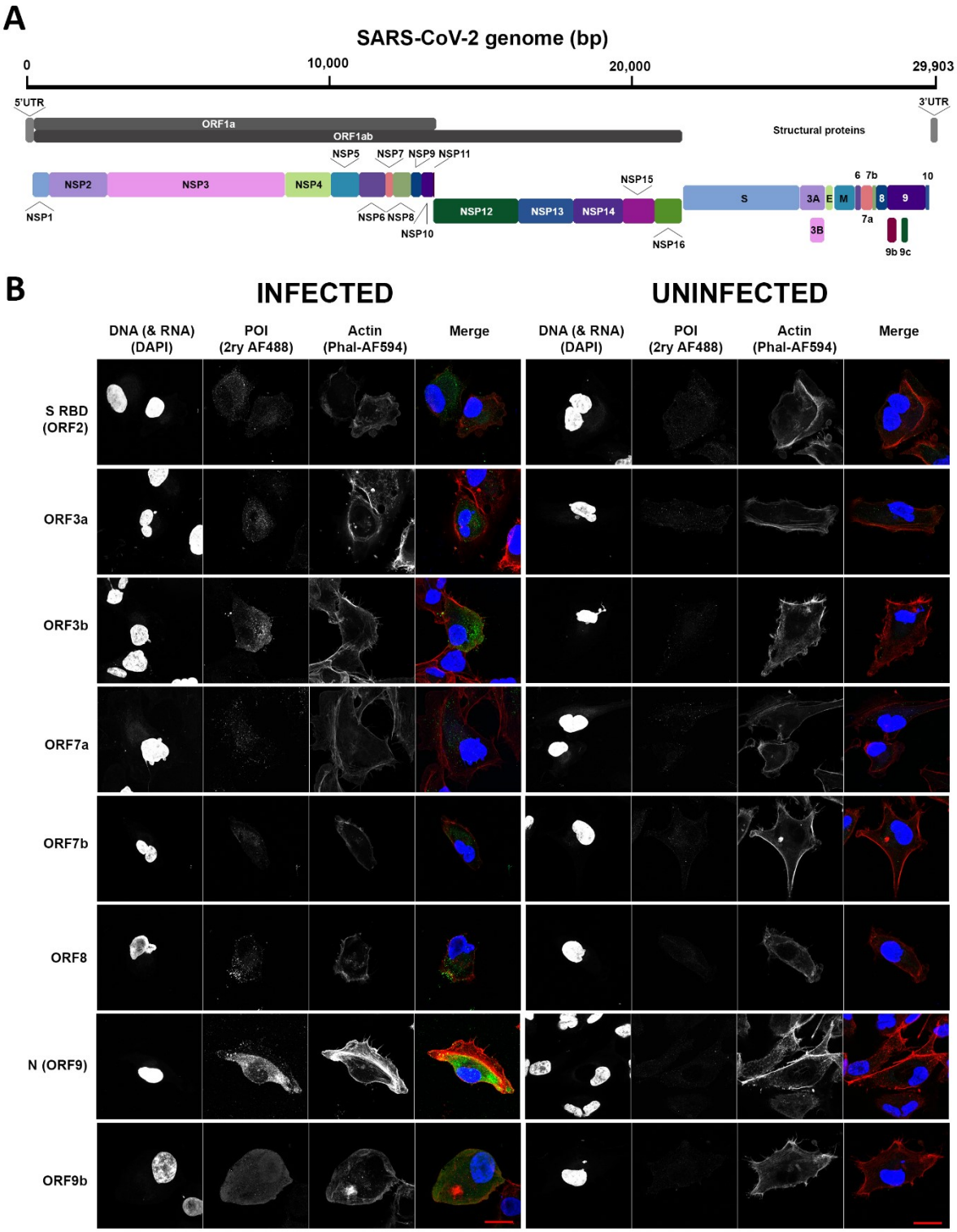

883

884

885 **Figure 3**

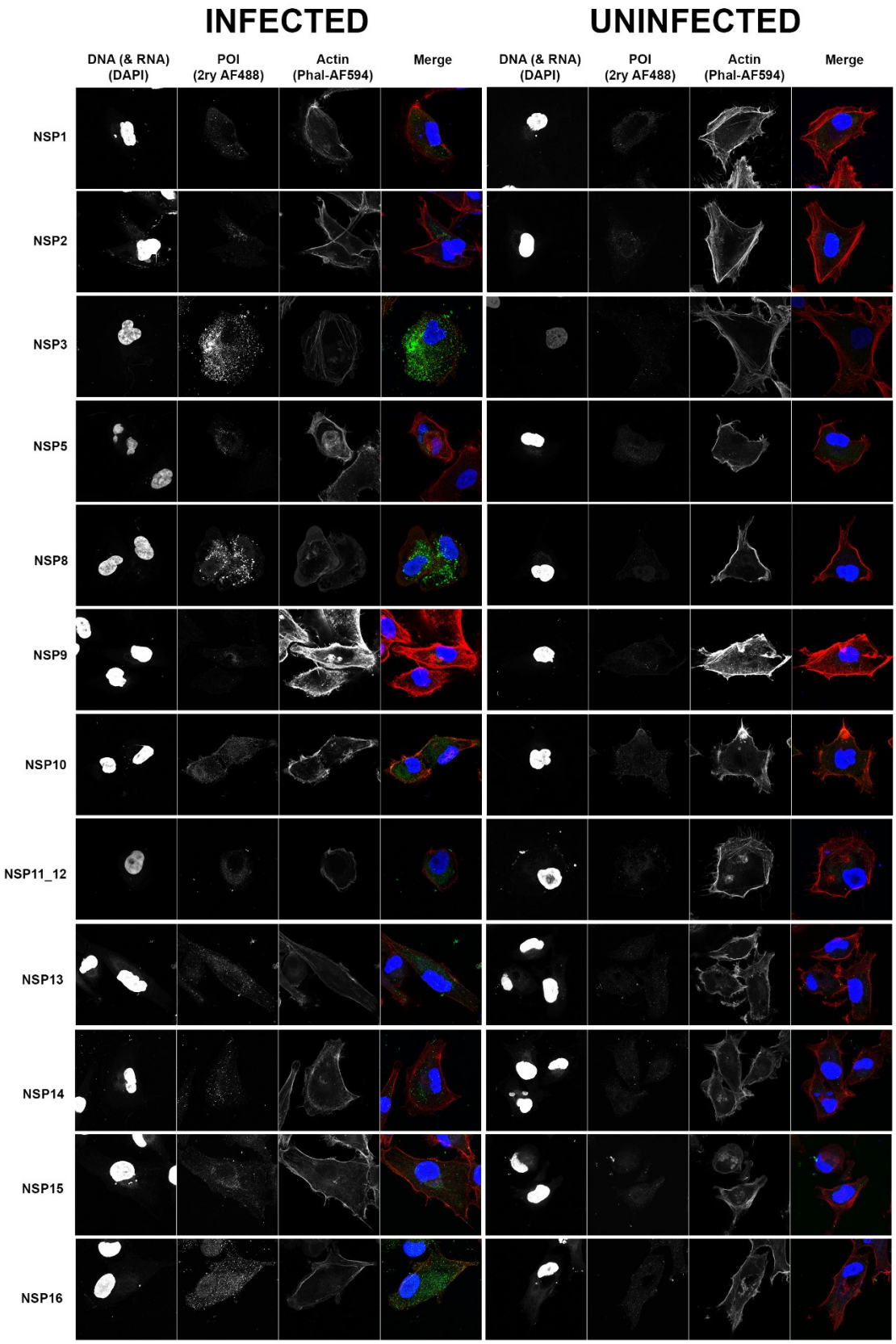

886

887 **Figure 4**

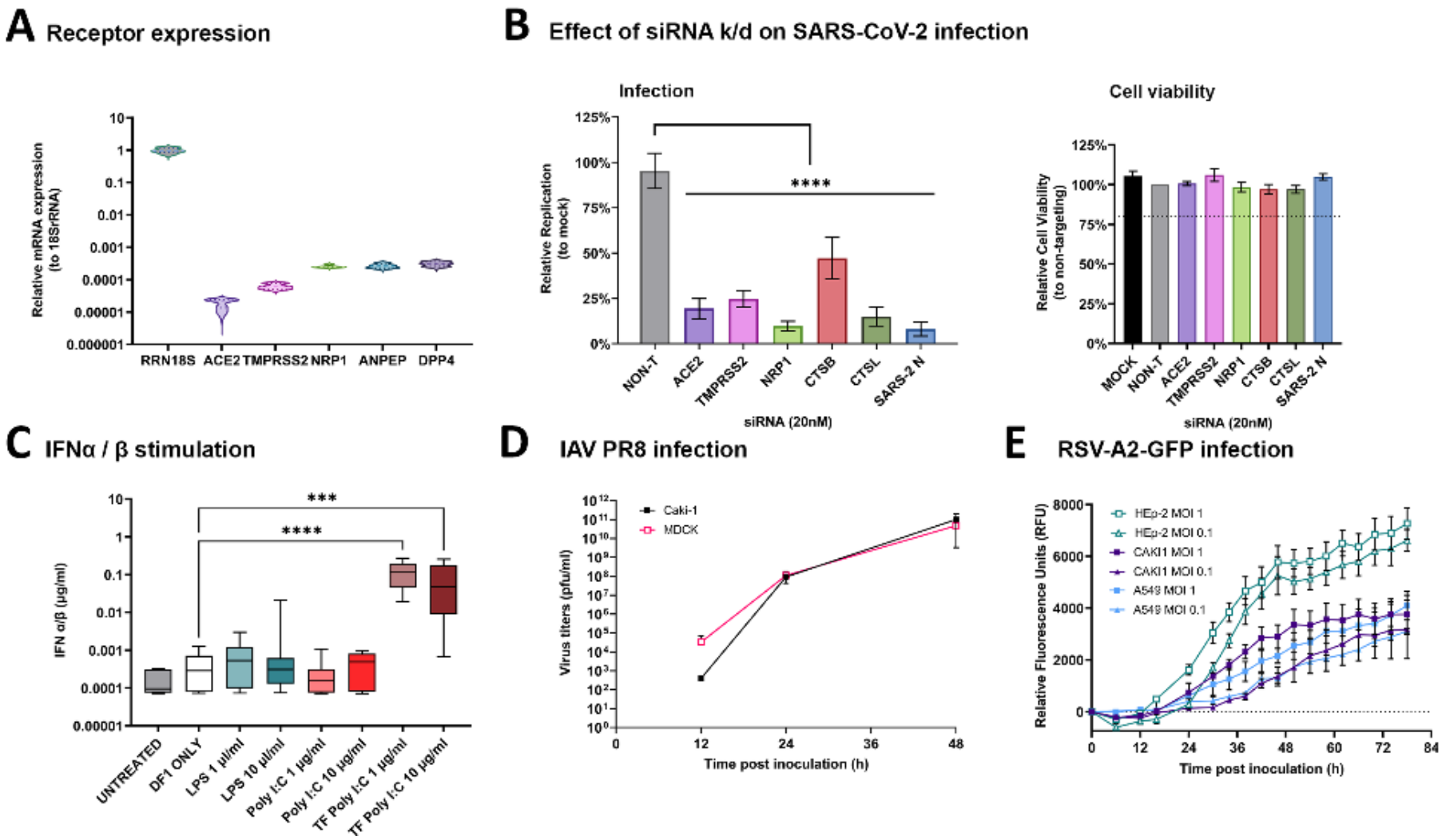

888